J. Fluid Mech. (1994), *vol.* 273, *pp.* 189–211

Movement of magnetic bacteria in time-varying magnetic fields

By BERNHARD STEINBERGER[1]†, NIKOLAI PETERSEN[1], HARALD PETERMANN[2] AND DIETER G. WEISS[3]

[1] Institut für Geophysik, Ludwig-Maximilians-Universität München, Theresienstr. 41, D-80333 Munich, Germany

[2] Fachbereich Geowissenschaften, Universität Bremen, D-28334 Bremen, Germany

[3] Tierphysiologie, Universität Rostock, Universitätsplatz 2, D-18051 Rostock, Germany

(Received 3 September 1990 and in revised form 25 February 1994)

The magnetic moment of individual living magnetic bacteria was determined by motion analysis in a time-dependent magnetic field. For this purpose we had to estimate the drag exerted on the moving bacterium by the surrounding liquid. First, the bacterium was approximated by an ellipsoid. In order to determine drag coefficients for more complicated (and realistic) forms, a model experiment was built. In this experiment enlarged models of bacteria were rotated in a viscous liquid and the torque acting upon them was measured. Computing algorithms were developed in order to calculate drag coefficients of magnetic bacteria and to simulate their motion in magnetic fields. The experimental and numerical determination of the drag coefficients agree within their error bounds. Besides the determination by motion analysis, the bacterial magnetic moment was also calculated from the number and size of magnetic particles contained in the bacterium as seen in an electron microscope. The results of both calculations agree well.

1. Introduction

Magnetic bacteria were discovered by Blakemore (1975). In contrast to other bacteria, magnetic bacteria have a magnetic dipole moment caused by chains of tiny, submicroscopic magnetite particles – called magnetosomes by Balkwill, Maratea & Blakemore (1980) – inside the bacterium.

In the ambient Earth's magnetic field the swimming bacteria are passively oriented like a compass needle and then move automatically along the field lines by self-propulsion. The direction of the magnetic moment is such that the bacteria always swim downwards. This enables them to swim straight downwards to the sediment layer which provides the most favourable living conditions, when they have been whirled up from the ground.

Rather than being a rarity of nature, magnetic bacteria are widespread in both marine and freshwater environments (Moench & Konetzka 1978; Towe & Moench 1981; Blakemore 1982; Spormann & Wolfe 1984; Sparks *et al.* 1986; Oberhack & Süssmuth 1987; Farina, Lins de Barros & Esquivel 1988; DeLong, Frankel & Bazylinski 1993). They exist in both the northern and southern hemispheres and also near the equator (Kirschvink 1980; Blakemore, Frankel & Kalmijn 1980; Frankel *et al.* 1981).

† Present address: Department of Earth and Planetary Sciences, Hoffman Laboratory, Harvard University, 20 Oxford Street, Cambridge MA 02138, USA.

For our study we used magnetic bacteria from lakes in the Alpine foreland of Southern Germany. Here the habitat of the magnetic bacteria comprises the uppermost 2 cm of the sediment, with a maximum population density of approximately 10^7/ml occurring at a depth of 2–10 mm below the water/sediment interface. This zone is characterized by an O_2-concentration approaching zero.

A large variety of different forms of magnetic bacteria was found, including spirilli, cocci, vibrios, and rod-shaped bacteria. The phylogenetic relationship for some of these types has been established by Spring *et al.* (1992) by analyses of subunits of ribosomal RNA sequences.

The aim of this study is to calculate the swimming path of magnetic bacteria in varying magnetic fields and subsequently to deduce their magnetic moment from motion analysis.

2. Methods of determining the magnetic moment of magnetic bacteria

Assuming that all magnetosomes within a bacterium are single-domain magnetite particles and that the magnetic moments are aligned parallel to the long axis of the particle chain, the total moment of a bacterium can be calculated from the size and number of the magnetosomes as determined by electron microscopy. For the type of bacterium shown in figure 1 a magnetic moment of the order of magnitude of 10^{-12} G cm^3 was thus obtained.

The obvious disadvantage of this method is that certain assumptions have to be made on the alignment of the magnetic moments of the individual magnetosomes. We therefore applied a different method which determines the bacterial magnetic moment independently of electron microscopy from the analysis of the movement of the bacterium in rotating magnetic fields (Petersen, Weiss & Vali 1989).

In a constant homogeneous magnetic field the forward speed of a magnetic bacterium is given by the balance between its propulsive force and the opposing viscous drag. In a rotating magnetic field however, a magnetic torque is also acting, which causes the bacterium to rotate in addition to its forward movement. The bacterium then swims in a circle (figure 2*b*). Without a rotating magnetic field the bacteria swim straight ahead (figure 2*a*). They are presumably only passively turned by the magnetic field. Because we have conditions of Stokes flow (see below), the linearity of the equations allows us to treat the rotation independently of the forward motion to the extent that the resistance factor and orientation of the bacterium are unaffected by movements.

The rate of rotation of the bacterium is given by the balance between the magnetic torque and an opposing viscous drag, the latter increasing with rotational speed. The instantaneous direction of the magnetic moment μ of the bacterium is not parallel to the applied rotating field H, the direction of the moment lagging behind that of the field by an angle (μ, B) so as to give a torque $\boldsymbol{\mu} \times \boldsymbol{B}$, of magnitude $\mu B \sin(\mu, B)$, which tries to rotate the bacterium to be more parallel to B.

As bacteria are so small (approximately 1–10 μm) their hydrodynamics is described by a very low Reynolds number (Purcell 1977). For a typical length $l_0 = 6$ μm, a typical swim velocity $v_0 = 30$ μm s^{-1} and the kinematic viscosity of water $\nu = 10^{-6}$ m^2 s^{-1}, we obtain a Reynolds number

$$Re = v_0 l_0 / \nu = 1.8 \times 10^{-4}.$$

Therefore, in order to describe the motion of the liquid around the bacterium, the Navier–Stokes equation can be substituted by the (linear) Stokes equation. That

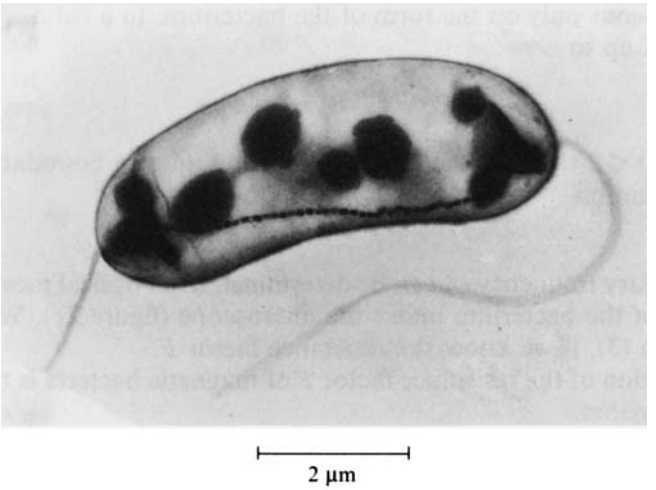

FIGURE 1. Magnetic bacterium from Lake Chiemsee (Southern Germany) with a single chain of prismatic magnetosomes aligned along its axis. The bacterium was sampled from the uppermost 2 cm of the sediment in a water depth of 20 m. For TEM observation the bacterium was fixed with 2.5% glutaraldehyde in a 0.1 M cacodylate buffer (pH 7.2), rinsed with water and stained with 2% uranyl acetate solution. Electronmicrograph by H. Vali.

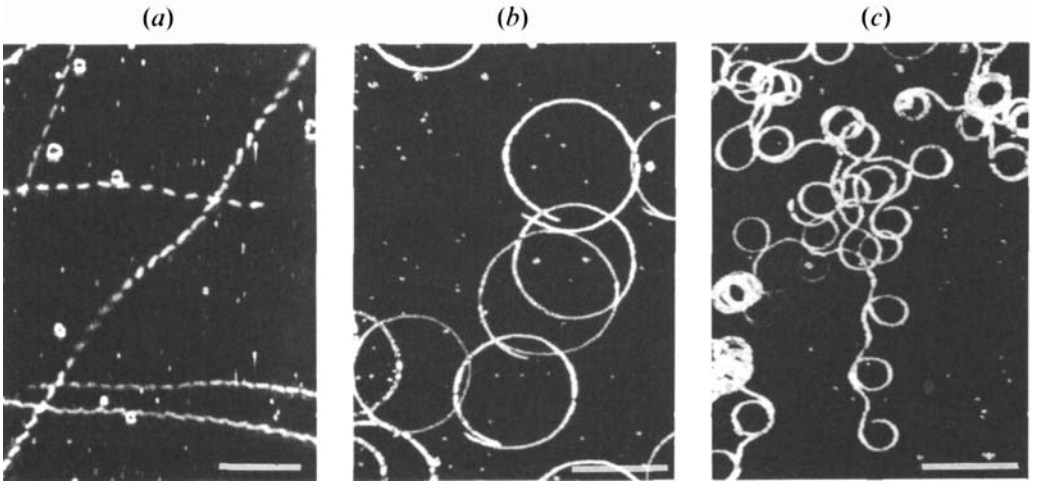

FIGURE 2. Swimming tracks of magnetic bacteria in different rotating magnetic fields. The bacteria were recorded under a light microscope with a video camera. The recorded sequences were digitally processed with a real-time image processor; to visualize the tracks the built-in real-time function 'trace' was used. (*a*) Zero magnetic field: the bacteria move straight but in different directions. (*b*) Rotating magnetic field: the bacteria move in circles (field strength $H = 1.6$ Oe, rotation period $T = 10$ s). (*c*) Rotating magnetic field: here the viscous forces dominate the swimming behaviour, the period T is too short and the bacteria cannot follow the field, they 'break out'. $H = 1.6$ Oe, $T = 2.5$ s. Bars 50 μm.

means, in the case described above, a linear relationship between magnetic torque M and angular velocity ω:

$$M = -\eta F \omega. \tag{1}$$

Here η is the (constant) viscosity of the surrounding liquid and F is the scalar resistance

factor, which depends only on the form of the bacterium. In a rotating magnetic field both torques add up to zero:

$$\mu B \sin(\mu, B) = -\eta F \omega. \tag{2}$$

Because $\sin(\mu, B) \leqslant 1$ the bacterium can only rotate up to a boundary frequency ω_b, for which the equation

$$\mu B = \eta F \omega_b \tag{3}$$

holds. The boundary frequency ω_b can be determined from optical measurement of the swimming path of the bacterium under the microscope (figure 2*c*). We can therefore determine μ from (3), if we know the resistance factor F.

The determination of the resistance factor F of magnetic bacteria is therefore a main objective of this paper.

3. Calculation of resistance factors and simulation of the movement of magnetic bacteria

3.1. *The concept of resistance tensors*

The force $\boldsymbol{K}$ and torque $\boldsymbol{M}$ which act upon a bacterium are related linearly to its forward speed $\boldsymbol{v}$ and angular velocity $\boldsymbol{\omega}$ (and, if there is any, the angular velocity of the flagella relative to the body of the bacterium). More generally than (1) this can be written for a rigid body as

$$\left.\begin{aligned} \boldsymbol{K} &= -\eta(\boldsymbol{F}_{11}\cdot\boldsymbol{v}+\boldsymbol{F}_{12}\cdot\boldsymbol{\omega}) = 0, \\ \boldsymbol{M}_{vis} &= -\eta(\boldsymbol{F}_{21}\cdot\boldsymbol{v}+\boldsymbol{F}_{22}\cdot\boldsymbol{\omega}) = -\boldsymbol{M}_{mag} \end{aligned}\right\} \tag{4}$$

(Happel & Brenner 1965, Chap. 5). No net force acts on the body and the magnetic torque balances the viscous torque.

$\boldsymbol{F}_{11}$, $\boldsymbol{F}_{12}$, etc. are tensors, which only depend on geometry. They are called *resistance tensors*. Real bacteria however have flagella, which rotate relative to the body and thus propel the bacterium. For reviews on bacterial locomotion and flagellar propulsion see Wu, Brokaw & Brennen (1975). If we consider this, we obtain

$$\left.\begin{aligned} \boldsymbol{K} &= -\eta\left(\boldsymbol{F}_{11}\cdot\boldsymbol{v}+\boldsymbol{F}_{12}\cdot\boldsymbol{\omega}+\sum_{i=1}^{n}\boldsymbol{F}_{12,i}^{rel}\cdot\boldsymbol{\omega}_i^{rel}\right) = 0, \\ \boldsymbol{M}_{vis} &= \eta\left(\boldsymbol{F}_{21}\cdot\boldsymbol{v}+\boldsymbol{F}_{22}\cdot\boldsymbol{\omega}+\sum_{i=1}^{n}\boldsymbol{F}_{22,i}^{rel}\cdot\boldsymbol{\omega}_i^{rel}\right) = -\boldsymbol{M}_{mag} \end{aligned}\right\} \tag{5}$$

instead of (4). Here $\boldsymbol{\omega}_i^{rel}$ is the angular velocity of the flagellum (or bundle of flagella) i relative to the body; n is the number of the flagella or bundles ($n = 1$ or 2).

In the most simple cases (e.g. an ellipsoid rotating around one of its axes of symmetry), a torque $\boldsymbol{M}$ will only lead to a rotation with $\boldsymbol{\omega} \parallel \boldsymbol{M}$ and we can therefore directly obtain a scalar resistance factor F. If this is not possible, we invert (4) or (5) for $\boldsymbol{v}$ and $\boldsymbol{\omega}$. By numerical integration we calculate the movement of the bacterium in a magnetic field and for a given magnetic moment. Then we obtain in particular the boundary frequency. Using (3) we can thus calculate a scalar 'apparent resistance factor'. With this apparent resistance factor, we can still apply (3) to determine the magnetic moment.

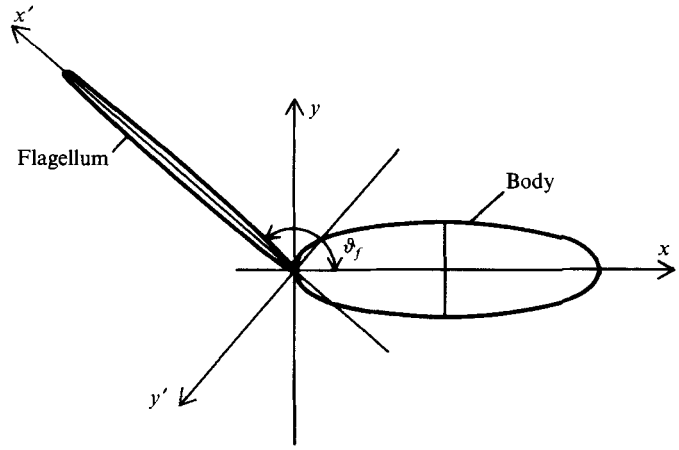

FIGURE 3. Model of a planar bacterium. In the special case $\vartheta_f = 180°$ we have the model of a linear bacterium.

In (4) and (5), $\boldsymbol{M}_{vis}$ refers to an arbitrarily chosen point and $\boldsymbol{v}$ refers to the same point. Since $\boldsymbol{\omega} \times (\boldsymbol{r}-\boldsymbol{r}_1) = \boldsymbol{\omega} \times (\boldsymbol{r}-\boldsymbol{r}_0) + \boldsymbol{\omega} \times (\boldsymbol{r}_0-\boldsymbol{r}_1)$, a rotation about a point $\boldsymbol{r}_1$ with $\boldsymbol{\omega}$ is equivalent to a rotation about a point $\boldsymbol{r}_0$ with $\boldsymbol{\omega}$ combined with a translatory movement with $\boldsymbol{v} = \boldsymbol{w} \times (\boldsymbol{r}_0-\boldsymbol{r}_1)$. Thus $\boldsymbol{v}$ and consequently the resistance tensors are also arbitrary. So we have to be clear about our point of reference.

3.2. *Methods for calculating resistance factors*

3.2.1. *The method using ellipsoid formulae*

There exist analytical formulae for the resistance factors of spheres and ellipsoids. For translatory motion these are given by Oberbeck (1876), and for rotation they are given by Jeffery (1922).

From these sources we calculate the following resistance tensor elements for a prolate ellipsoid of revolution with a long semiaxis a in the x-direction and short semiaxes b in the y- and z-directions:

$$F_{11}^{xx} = \frac{16\pi}{q_0 + \alpha_0 a^2}, \quad F_{11}^{yy} = F_{11}^{zz} = \frac{16\pi}{q_0 + \beta_0 b^2}, \quad F_{22}^{xx} = \frac{16\pi}{3\beta_0}, \quad F_{22}^{yy} = F_{22}^{zz} = \frac{16\pi(b^2+a^2)}{3(b^2\beta_0 + a^2\alpha_0)}.$$

All other elements are zero. In the above,

$$q_0 = -\frac{1}{e}\ln\frac{a-e}{a+e}, \quad \alpha_0 = -\frac{2}{e^2 a} - \frac{1}{e^3}\ln\frac{a-e}{a+e}, \quad \beta_0 = \frac{a}{e^2 b^2} + \frac{1}{2e^3}\ln\frac{a-e}{a+e};$$

$e := (a^2-b^2)^{1/2}$ is the eccentricity.

We used these formulae to calculate resistance factors of bacteria, which consist of two or three prolate ellipsoids of revolution rigidly connected: one ellipsoid for the body, and a very thin ellipsoid for a flagellum or a bundle of flagella at one end or at either end. However, we cannot consider the mutual interaction of the ellipsoids with this concept. The interaction of body and flagellum was studied by Higdon (1979), but his analysis is confined to the case of a spherical cell body. We do not want to restrict ourselves to such a special geometry and therefore neglect the interaction.

Dimensionless quantity	For real bacteria in water	For model bacterium in glycerol
Independent		
Viscosity 1	10^{-3} kg m^{-1} s^{-1}	1 kg m^{-1} s^{-1}
Length 1	1 μm [2 μm]	1 cm
Time 1	1 s	—
B-field 1	0.1 G	—
Dependent		
Resistance factor 1	1 μm^3 [8 μm^3]	1 cm^3
Magnetic moment	10^{-12} G cm^3 [8×10^{-12} G cm^3]	—

TABLE 1. Conversion from dimensionless to dimensional quantities

We considered two special cases with two ellipsoids: in the 'linear case' the long axes of both ellipsoids are parallel to each other and orthogonal to the torque; in the 'planar case' both long axes of the ellipsoids are orthogonal to the torque, but not necessarily parallel to each other. Both special cases (see figure 3) can be described by a scalar resistance factor.

3.2.2. *Slender-body theory*

With the slender-body theory we can approximately calculate the viscous drag of a body that is much longer than it is broad. This is the case for a flagellum, or if flagella combine in a bundle (e.g. see Jarosch 1967; Macnab & Ornston 1977). With a greater error we can also apply it to the body of a bacterium.

According to Keller & Rubinow (1976) the zeroth approximation $\boldsymbol{\alpha}^{(0)}(s)$ to $\boldsymbol{\alpha}(s)$ (the force per length divided by $-8\pi\eta$) is given by

$$\boldsymbol{\alpha}^{(0)}(s) = \frac{1}{4\ln a(s)}[2\boldsymbol{I}-\boldsymbol{i}(s)\,\boldsymbol{i}(s)]\cdot\{\boldsymbol{u}_0(s)-\boldsymbol{v}(s)\}. \tag{6}$$

The first iterate $\boldsymbol{\alpha}^{(1)}(s)$ is

$$\begin{aligned}\boldsymbol{\alpha}^{(1)}(s) = \boldsymbol{\alpha}^{(0)}(s) &+ \frac{1}{4\ln a(s)}[2\boldsymbol{I}-\boldsymbol{i}(s)\,\boldsymbol{i}(s)]\cdot\{\alpha_2^{(0)}(s)\boldsymbol{j}+\boldsymbol{\alpha}^{(0)}(s)\ln[4s(1-s)]\\ &+\alpha_1^{(0)}(s)\,\boldsymbol{i}(s)[\ln(4s(1-s))-2]\\ &+\int_{-s}^{1-s}\left[\frac{\boldsymbol{\alpha}^{(0)}(s+t)}{R_0}-\frac{\boldsymbol{\alpha}^{(0)}(s)}{|t|}+\frac{\boldsymbol{R}_0\,\boldsymbol{R}_0\cdot\boldsymbol{\alpha}^{(0)}(s+t)}{R_0^3}-\frac{\alpha_1^{(0)}(s)\,\boldsymbol{i}(s)\,t^2}{|t|^3}\right]\mathrm{d}t.\end{aligned} \tag{7}$$

Here, $\boldsymbol{r}=\boldsymbol{r}_0(s)$, $0\leqslant s\leqslant 1$, is the centreline C of an oblong body of length 1, with a circular cross-section but otherwise arbitrary shape, with s being the arclength along C; $\boldsymbol{v}(s)$ is the translational velocity of the body surface at s, $\boldsymbol{u}_0(s)$ is the fluid velocity in the absence of the body at the point $\boldsymbol{r}_0(s)$, and $a(s)\ll 1$ is the radius of the body cross-section at s.

Also, $\boldsymbol{R}_0=\boldsymbol{r}_0(s)-\boldsymbol{r}_0(s+t)$, $\boldsymbol{I}$ is the unit matrix, $\boldsymbol{i}(s)$ is the unit vector tangential to C, $\boldsymbol{j}$ is the unit vector in the direction of the component of $\boldsymbol{u}_0(s)-\boldsymbol{v}(s)$ perpendicular to $\boldsymbol{i}$, α_1 is the component of $\boldsymbol{\alpha}$ in the direction of $\boldsymbol{i}$, and α_2 is the component of $\boldsymbol{\alpha}$ in the direction of $\boldsymbol{j}$.

Keller & Rubinow (1976) state that their result for the first iterate of the force per

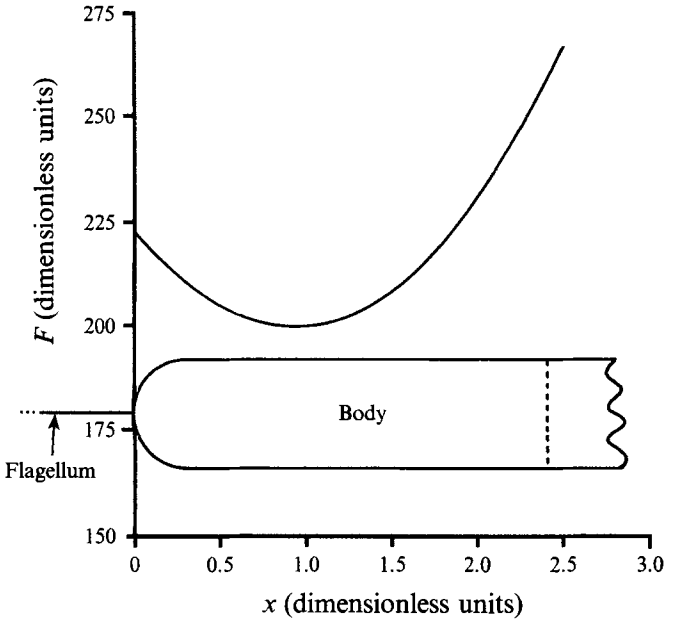

FIGURE 4. Resistance factor F of a linear model bacterium (see text and figure 3) as a function of the x-coordinate of the centre of rotation. The rotation axis is in the z-direction. Calculations were done with the ellipsoid formulae.

length agrees with the result of Cox (1970), although the latter is in a quite different form. Other treatments of slender-body theory are given by Batchelor (1970), Cox (1971) and Tillet (1970). However, these publications deal with the more special cases of an axisymmetric (Cox 1971; Tillet 1970), or at least straight (Batchelor 1970) slender body. Since we do not confine ourselves to these special cases, we find it most convenient to apply the formulae obtained by Cox (1970) and Keller & Rubinow (1976) in all our calculations.

By integration we can calculate the total force and the total torque, related to an arbitrary point on the body. By doing this for six special movements of the body (three translations and three rotations) we can calculate the resistance tensors of a body of length 1. These can be scaled to any length l_0 by multiplying $\boldsymbol{F}_{11}$ by l_0, $\boldsymbol{F}_{12}$ and $\boldsymbol{F}_{21}$ by l_0^2 and $\boldsymbol{F}_{22}$ by l_0^3.

3.3. *Results*

In the following we describe numerical results (and corresponding experimental results in the next section) for various shapes. In all calculations we chose dimensionless units. Table 1 shows several ways of converting from dimensionless to dimensional quantities. The first four conversions may be chosen arbitrarily, the other conversions then depend on these.

The numerical values in this section were chosen to make comparison with the model experiment of §4 particularly easy, using table 1 for conversion. The models there are meant to be roughly scaled images of real bacteria. The exact dimensions depend on the manufacturing process and have no particular significance.

The first example shows the resistance factor of a bacterium as a function of the position of the rotation axis (figure 4). The bacterium consists of an ellipsoid of revolution with length 4.79 and diameter 0.62 ('body') and another ellipsoid of revolution with length 4.79 and diameter 0.01 ('flagellum'). For convenience we will

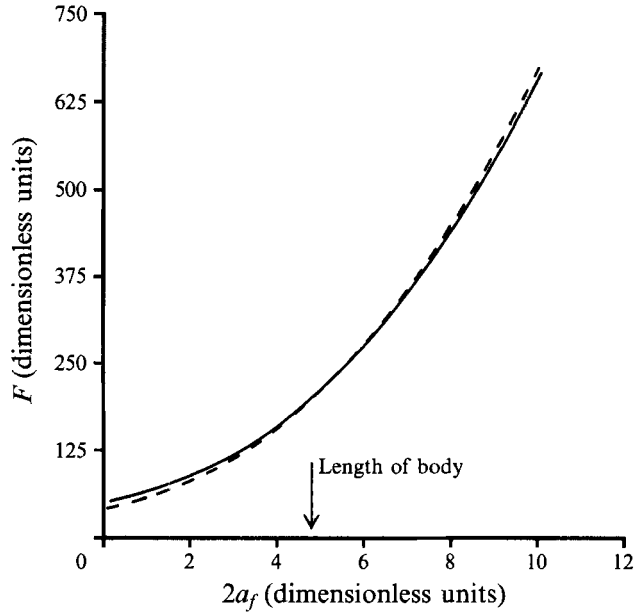

FIGURE 5. Resistance factor F for a linear bacterium (see figure 3), rotating around its centre of 'free' rotation as function of the length of the flagellum $2a_f$. The body has the same dimensions as model bacterium 1 and the flagellum has the diameter 0.01. The rotation axis is in the z-direction. Continuous lines were calculated with the ellipsoid formulae, dashed lines with slender-body theory.

call this 'model bacterium 1' (these dimensions were chosen to facilitate the comparison with the model bacterium of §4). The minimum torque occurs at the centre of 'free' rotation $(x, y) = 0.931$, i.e. when there is no external force applied.

Figure 5 shows an example of how the scalar resistance factor depends on the length of the flagellum. If the flagellum has a length of 4.79 (same length as the body) $F = 200$ results, compared to $F = 314$ for an ellipsoid of double length (i.e. length 9.58, diameter 0.62). The latter value would be expected if the bacterium had a whole bundle of flagella as wide as the body. Both values do not differ too much, whereas the resistance factor strongly depends on the length of the flagellum.

In figure 6(a, b) we show an example of how the scalar resistance factor depends on the angle ϑ_f between the body and flagellum. In figures 5 and 6 the continuous lines were obtained by using the ellipsoid formulae. The dashed lines we obtained with slender-body theory.

The ellipsoid formulae yield higher torques than slender-body theory for small angles ϑ_f, probably because we neglect the interaction between body and flagellum: each of these reduces the torque acting on the other. In the extreme case of the rotation of two thin ellipsoids next to each other, the torque is only slightly greater than for a single ellipsoid.

Next we considered a more realistic model bacterium, which consists of an ellipsoidal body of length 4.79 and diameter 0.62 and a flagellum, which looks similar to a helix, but is bent towards the centreline at one end where it touches the body. The axis length of the helix is 4.79, the wavelength is also 4.79, the diameter of the helix is 2.08, and the diameter of the cord is 0.01. For convenience we will call a bacterium with these dimensions 'model bacterium 2'. For the body we used the ellipsoid formulae, for the flagellum the slender-body theory. The mutual interaction was neglected.

Figure 7(a, b) shows the motion of a 'dead' magnetic bacterium (i.e. with no relative

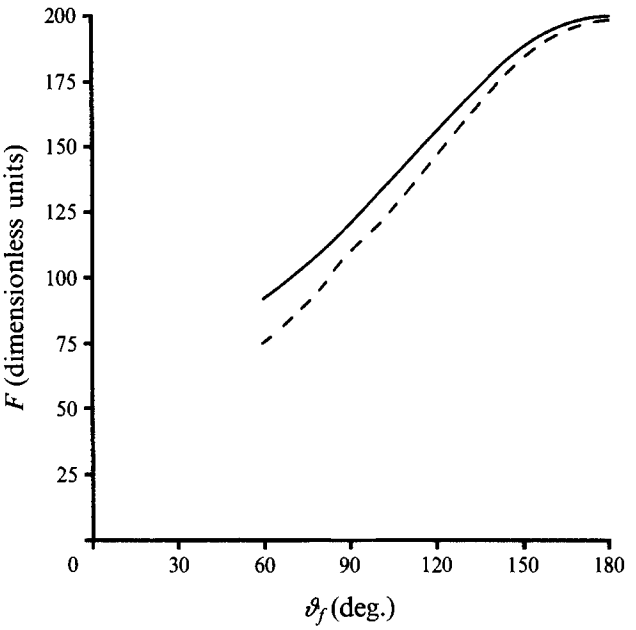

FIGURE 6. Resistance factor F for a planar model bacterium 1 (see figure 3), rotating around its centre of 'free' rotation as a function of the angle ϑ_f between body and flagellum, which varies between 180° and 60°. The rotation axis is in the z-direction. These angles correspond to the end points of the curves. Continuous lines were calculated with the ellipsoid formulae, dashed lines with slender-body theory.

rotation of body and flagellum and no forward motion) in a rotating magnetic field. For an angular frequency of the B-field $\omega_B = 0.113$, the bacterium can follow the rotation (figure 7*a*). The phase difference between the magnetic moment and the magnetic field converges towards approximately 79°. Therefore the magnetic torque is $\mu B \sin 79°$. We conclude that the boundary frequency ω_b is close to $0.113/\sin 79° \approx 0.115$. In figure 7(*b*) with $\omega_B = 0.13$ the bacterium cannot follow the rotation of the magnetic field any more, but tilts in the direction of the z-axis.

The reason for this behaviour can be explained as follows. When the angle between the magnetic field and the magnetic moment becomes greater than 90° the direction of the magnetic moment in the (x, y)-plane becomes metastable. If the magnetic moment points somewhat out of the plane (because of thermal agitation or asymmetry of the bacterium) the magnetic field causes a torque which acts in a way that turns the magnetic moment further out of the plane. This effect becomes most pronounced, when the magnetic field and the magnetic moment point in nearly opposite directions.

A boundary frequency $\omega_b = 0.115$ corresponds to an apparent resistance factor of 219. With the model experiment described in the next section we could only determine the resistance tensor element F_{22}^{zz}. We call this the 'one-dimensional approximation'. For a model bacterium 2 in the (x, y)-plane we calculated, for different rotation angles of the axis of the helical flagellum, values of F_{22}^{zz} between 245 and 253. The difference in the value, which we obtained by the iteration above, gives an idea of how good the results of the model experiment are if there are no other sources of error.

The next example in figure 8(*a–c*) shows some trajectories of living magnetic bacteria, i.e. with relative rotation of body and flagellum, in a magnetic field (magnetic field intensity here is 50 × the one chosen for the dead bacterium). For $\omega_B = 5$ (figure

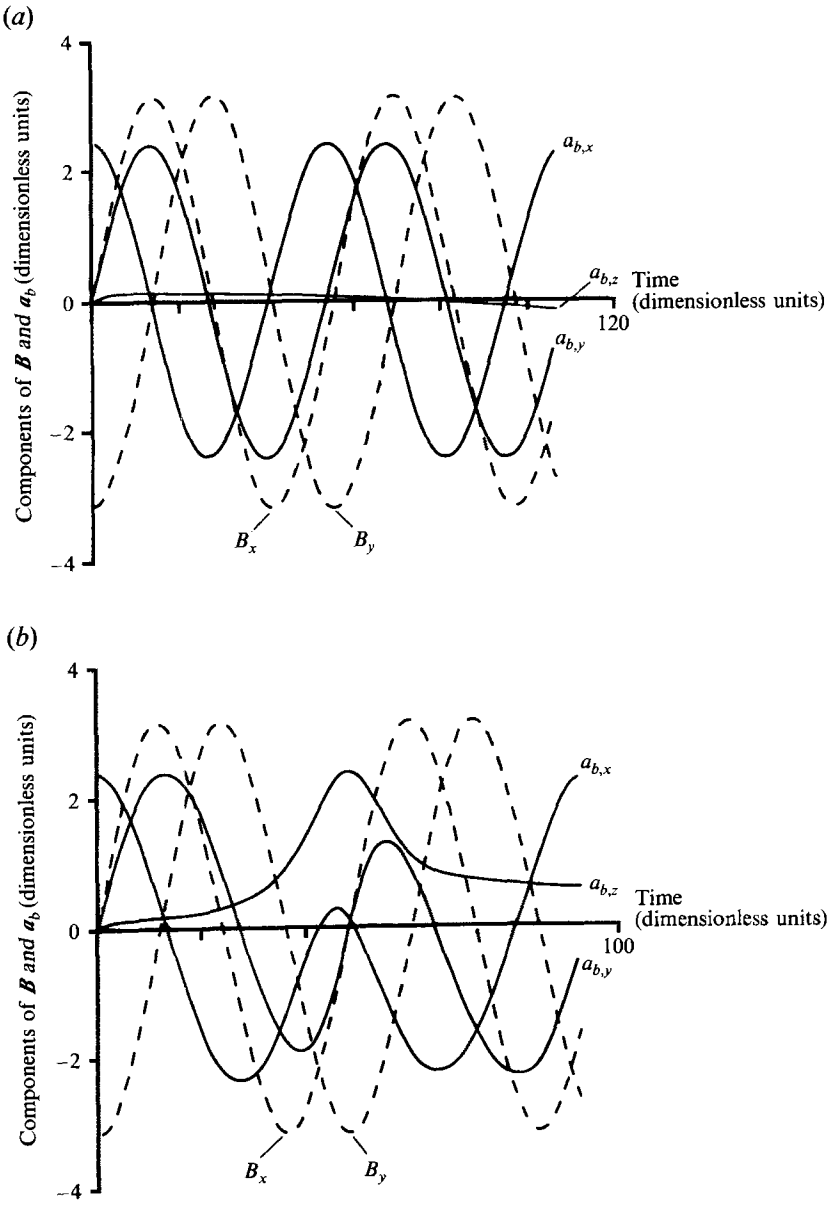

FIGURE 7. Components of the magnetic field $\boldsymbol{B}$ and the vector $\boldsymbol{a}_b$ which represents the long half-axis of the body of the bacterium and points away from the flagellum as a function of time, for a 'dead' model bacterium 2. The angle between body and axis of the helix of the flagellum is $\vartheta_f = 140°$. The magnetic moment is 8 and points in $-\boldsymbol{a}_b$-direction. The viscosity of the surrounding liquid is 1. (*a*) Angular frequency of the magnetic field $\omega_B = 0.113$, and (*b*) $\omega_B = 0.130$.

8*a*) the trajectory converges approximately towards a circle in the (x, y)-plane. The slow movement in the z-direction is probably due to the asymmetry of the bacterium. The bacterium can follow the rotation of the field and the calculated trajectory agrees with what one expects and observes (see figure 2*a*).

For $\omega_B = 5.25$ (figure 8*b*), the trajectory spirals around the z-axis because the body again tilts. This means a reduction of the viscous drag for rotation around the z-axis.

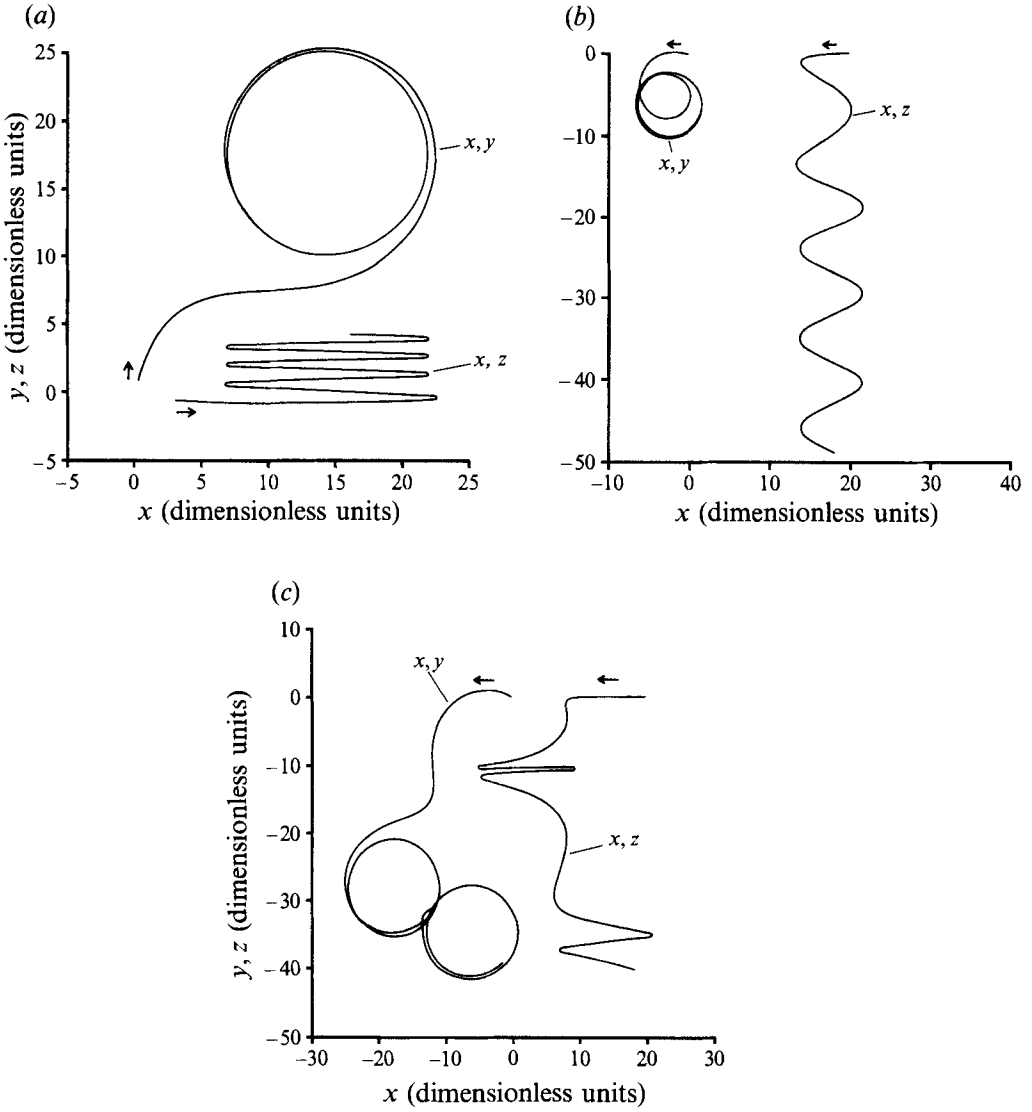

FIGURE 8. Trajectories of a 'living' magnetic bacterium for different angular frequencies of the rotating magnetic field. The flagellum points ahead in the direction of motion and rotates 100 times per time unit. The magnetic field (intensity = 50π) rotates in the (x, y)-plane. Otherwise as in figure 7. The arrows indicate the direction of motion. Projections of the trajectory (of the centre of the body) into the (x, y)-plane and into the (x, y)-plane (if necessary shifted sidewards) are shown. (*a*) $\omega_B = 5$, (*b*) $\omega_B = 5.25$, (*c*) $\omega_B = 6$.

We can then reach a new equilibrium with an angle of exactly 90° between the magnetic moment and the magnetic field, so that the bacterium neither tilts more nor is drawn back to the (x, y)-plane. The angle φ, by which the bacterium tilts, can be determined from the trajectory. One can calculate the boundary frequency ω_b approximately from the angle φ: $\omega_b = \omega_B/\cos\varphi$. In this case, we get $\omega_b = 5.24$, corresponding to an apparent resistance factor 240. If we divide ω_b by 50 (because of the 50-fold field intensity) we get a value which is lower by a factor 0.911 than for the dead bacterium. This is what we expect: one can show that the direction of the magnetic moment

approximately moves on a cone; if the cone angle is α, the maximum torque which can be provided on a time average is smaller by a factor $\cos\alpha$.

For $\omega_B = 6$ (figure 8*c*), the first part of the projection of the curve into the (x,y)-plane looks similar to what one observes under the microscope (see figure 2*b*), although the bacterium has already tilted here. If we neglect this latter effect we can explain this part of the trajectory as follows. The bacterium turns left because it tries to follow the magnetic field. However, because of the viscous drag it falls more and more behind, until the magnetic moment points in the direction opposite to the magnetic field. Then the movement changes to a right turn, because the torque changes sign; the magnetic field and the magnetic moment rotate towards each other until they are parallel; now the bacterium again turns left and so on. But then the effect of tilting becomes so pronounced that the bacterium mainly moves in the negative z-direction. This is not observed for real magnetic bacteria under the microscope. Because of the restrictions imposed by the glass walls of the slide and the cover glass, their movements are approximately confined to a plane. As soon as the boundary frequency is reached, their trajectories change from circles to the shape which we described above (see figure 2*c*).

Finally we considered how the torque, which acts on a rotating body, increases near a boundary. This is important as the bacteria under the microscope are usually near one of the boundaries. We calculated the resistance factor F for a cylinder which rotates around an axis orthogonal to the boundary and orthogonal to its axis of symmetry as a function of the distance δ to the boundary. We used the formulae, which are given by Yang & Leal (1983), in which the body is simply described by its radius (i.e. we essentially confine ourselves to cylindrical bodies). In our special case we obtain from these formulae (referring to the centre of the body) a resistance factor

$$F = \frac{8}{3}\pi l^3 \epsilon \left[1 - \epsilon\left(\ln 2 - \frac{11}{6} + \frac{3}{4l^3}\int_{-1}^{l} x^2 K(x,d)\,\mathrm{d}x\right)\right] + O(\epsilon^3). \tag{8}$$

Here,

$$\epsilon := \ln\left(\frac{2l}{R_0}\right),$$

$x :=$ integration parameter along the bacterium,

$d :=$ distance of the boundary,

$$K(x,d) := -\frac{1}{x}\{[l-x)^2+4d^2]^{1/2} - [(l+x)^2+4d^2]^{1/2}\} + B(x,d) + \frac{2d}{x}k(x,d),$$

$$k(x,d) := d\left[\frac{1}{[(l-x)^2+4d^2]^{1/2}} - \frac{1}{[(l+x)^2+4d^2]^{1/2}}\right],$$

$$B(x,d) := -g(x,d) - \tfrac{1}{2}h(x,d),$$

$$g(x,d) := \sinh^{-1}\frac{l-x}{2d} + \sinh^{-1}\frac{l+x}{2d},$$

$$h(x,d) := \frac{l-x}{[(l-x)^2+4d^2]^{1/2}} + \frac{l+x}{[(l+x)^2+4d^2]^{1/2}}.$$

$O(\epsilon^3)$ is a term of order ϵ^3.

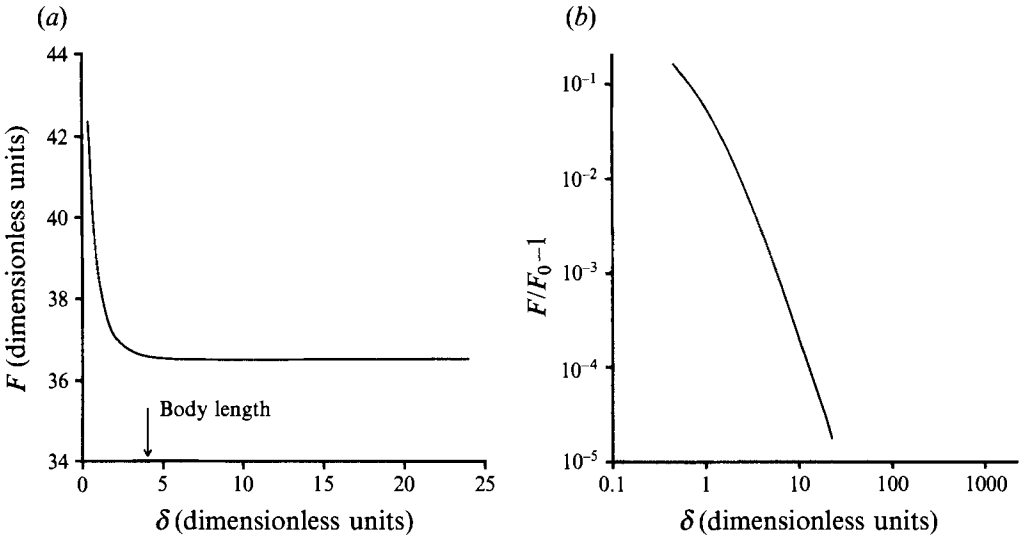

FIGURE 9(*a*, *b*). Calculated resistance factor F of a cylinder of length 4.1 and diameter 0.505 as a function of the distance δ of the centre of the cylinder to the horizontal boundary. The cylinder has a horizontal axis of symmetry and rotates around a vertical axis. F_0 is the resistance factor in an infinite viscous medium.

In figure 9(*a*, *b*) the result is shown for a length 4.1 and a diameter 0.505 (see also figure 1.1). According to this approximation, the deviation of the resistance factor from the limit for $\delta \to \infty$ is only 1%, if $\delta \approx 2.6$.

3.4. *Discussion of errors*

The total error that affects the theoretical determination of resistance factors and boundary frequencies comes from a combination of several errors. For each error we give in brackets our best guess.

(i) The error due to neglecting the interaction of several parts of the body. The magnitude of this error was estimated by calculating the velocity field of the liquid which surrounds a moving ellipsoid. Formulae are given by Oberbeck (1876) and Edwardes (1892). It was found to be a few percent for a straight body, and somewhat bigger for a bent one. (3% for a straight body, 10% for a bent one.)

(ii) The error of the slender-body approximation. This is at least 14%, if applied to the body; about 5% if applied to a straight flagellum; more, if the flagellum is bent because then the interaction among different parts will be represented only incompletely. The magnitude of the error was estimated by applying slender-body theory to ellipsoids, for which we have exact results for comparison. (14% for body only, 10% for body plus flagellum/a on one end, 9% for body plus flagellum on both ends.)

(iii) The error due to representation of non-ellipsoidal bodies by ellipsoids. (24% for body only – this value is the difference between the resistance factors of bodies (*a*) and (*c*) in figure 12, as obtained by slender-body theory, and 9% for body plus flagellum/a – this value is the difference between the resistance factors of body (*e*) in figure 12, and model bacterium 1 in §3.3, as obtained by slender-body theory.)

(iv) The error due to the effect of boundaries. (9% – see §4 for details.)

(v) The error due to the shape of the bacterium being only shown with some uncertainty, so that the model is only an imperfect image of the reality. If, for example,

the length of the flagellum is increased by 10% for model bacterium 1, the resistance factor increases by 13%. A 5% error in overall size causes a 16% error of the resistance factor. Therefore, with the present possibilities of observations, this error is of the same order of magnitude as the other errors, and our calculations are accurate enough. (16%.)

Assuming that the above errors are independent, we obtain the following estimates for the total error:

30%, if we use the ellipsoid formulae for the body only;

21%, if the bacterium is 'straight' and we use the ellipsoid formulae for body plus flagellum/a;

23%, if the bacterium is 'bent' and we use the ellipsoid formulae for body plus flagellum/a;

23%, 21% or 20%, if we use slender-body theory for the body only, for body plus flagellum/a on one end or on both ends respectively.

4. A model experiment for the determination of the scalar resistance factor of magnetic bacteria

4.1. *Experimental set-up*

A model experiment which determines the component of the torque in the z-direction for rotation of a model bacterium around the z-axis is useful if the error of the one-dimensional approximation is not too large and the Reynolds number is small enough.

We have seen in the last section that a one-dimensional approximation gives us a resistance factor which differs by only a few percent from the one we get for a three-dimensional calculation. As we shall see, an error of this order of magnitude is inherent to both the model calculations (see previous section) and the experiment; so the first condition is fulfilled well enough.

Our models are about 5 cm long and were spun with about 1 rotation per minute (i.e. $\omega \approx 0.1\ \mathrm{s}^{-1}$) in glycerol ($\nu \approx 10^{-3}\ \mathrm{m}^2\ \mathrm{s}^{-1}$). Therefore, we obtain a Reynolds number $Re \approx lu/\nu = l^2\omega/2\nu \approx 0.1$. This is much larger than for real bacteria, but even here inertial forces were not noticeable. If inertial forces were to play a noticeable role this would lead to a deviation from the linear relation between angular velocity and torque (see equation (1)), which we did not observe. Therefore, the second condition is fulfilled well enough.

The experimental set-up is shown in figure 10. It consists of three parts, which can rotate relative to each other (ideally around a vertical axis): the parts at rest in the laboratory, the revolving parts which are spun by the motor, and the parts which hang on a torsion thread.

The cylindrical container (at rest in the laboratory) has a diameter of about 44 cm and is 46 cm high. It is filled with glycerol and contains a second floor, whose height can be adjusted within the glycerol, so that one can vary the distance of the model from the solid boundary.

Above the container there is a platform with the revolving parts of the experiment. The most important revolving parts are: the galvanometer coil, mirror and model; the magnet, in the field of which the galvanometer coil is placed; the optical system fixed to the magnet.

On the torsion thread of the galvanometer the mirror, coil and model are suspended as one rigid unit. The model is fixed at the end of a thin ceramic rod and submerged in the glycerol. When the system is revolving a viscous torque is acting on the model which causes a deflection of the mirror. The deflection is then monitored via a light

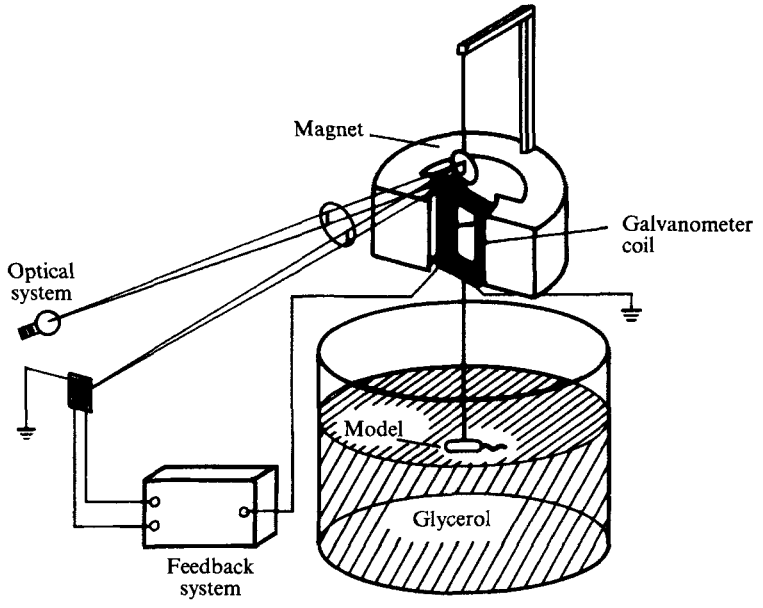

FIGURE 10. Schematic sketch of the model experiment.

beam by a photodiode. The resulting and amplified current is fed to the coil thus tuning a negative feedback. The feedback current is then a measure of the torque acting on the model.

4.2. *Results of the model experiment*

The results show how the resistance factor depends on the form of the body, the length and the form of the flagella, and the distance to a solid boundary. In order to calibrate the experiment, we used rotating spheres: for these the resistance factors can easily be calculated and so we could deduce the factor for the conversion of feedback current to resistance factor. This factor is strongly temperature dependent as it is proportional to the viscosity of the glycerol.

By changing the height of the second floor, we first determined experimentally the dependence of the resistance factor on the distance of the model from a solid boundary, which is (like a glass slide under the microscope) perpendicular to the rotation axis. The model used was a cylinder of diameter 0.505 cm and length 4.1 cm. In figure 11 (*a*, *b*) resistance factors are plotted against the distance from the centre of the model to the floor. From the logarithmic representations one can see that the resistance factor, as a function of distance δ to the boundary, may be fitted in the form

$$F = F_0(1+(\delta_0/\delta)^s), \quad s \approx 2, \quad F_0 = 48.82\ \text{cm}^3. \tag{9}$$

From figure 11 one can also see that the deviation of the resistance factor in an infinite liquid is only 1 % for $\delta \approx 4.6$ cm. In comparison we obtained computationally a deviation of 1 % for $\delta \approx 2.6$ cm (see figure 9). For $\delta = 4.6$ cm we get from our computation a deviation of only 0.3 % (i.e. the measured deviation is about three times larger than the computed one).

During our microscopic observation, the real bacteria are at least 2–4 μm away from the boundary. This corresponds to 0.8–1.6 cm in the model experiment as the scaling factor is about 4000. For this distance, the model experiment gave a deviation of between 38 % and 9 % from the value for the infinite liquid. However, the calculation yielded only a deviation of between 9 % and 2.8 %.

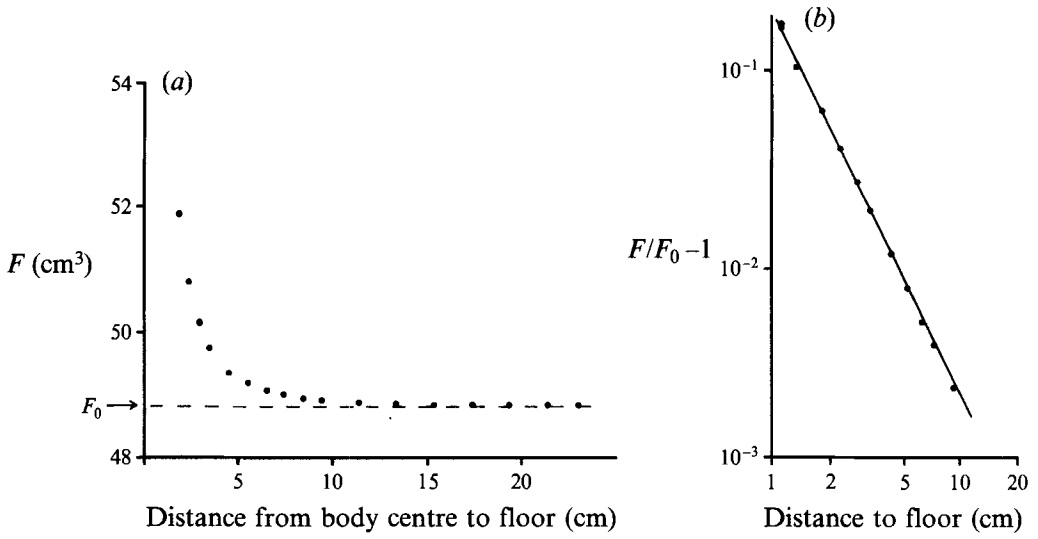

FIGURE 11(*a*, *b*). Measured resistance factor F of a cylinder (as in figure 9) for a solid boundary perpendicular to the rotation axis ('floor') as a function of the distance of the centre of the cylinder from the floor.

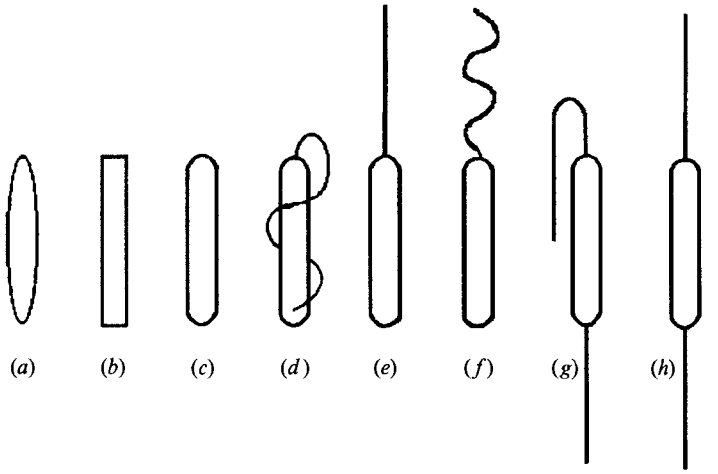

	(*a*)	(*b*)	(*c*)	(*d*)	(*e*)	(*f*)	(*g*)	(*h*)
Experimental results	–	1.52 ±0.16	1.40 ±0.14	1.60 ±0.16	4.90 ±0.50	5.70 ±0.58	6.01 ±0.61	10.28 ±1.02
Results by 2- or 3-ellipsoid theory	1.00	1.00 ±0.24	1.00 ±0.24	1.46 ±0.20	3.88 ±0.37	4.53 ±0.43	– –	8.98 ±0.82
Results by slender-body theory	0.88 ±0.12	1.13 ±0.16	1.09 ±0.15	1.01 ±0.14	4.24 ±0.42	4.67 ±0.47	– –	9.00 ±0.81

FIGURE 12. Resistance factors (with error estimates) for different bodies, divided by the resistance factor of an ellipsoid of the same length and diameter.

Next we measured resistance factors for a series of different bodies (see figure 12) and compared them with the respective theoretical results for ellipsoids of the same length and width (6.01 cm × 0.755 cm, resp. 4.79 cm × 0.62 cm):

(*a*) ellipsoid;

(*b*) cylinder of length 6.01 cm, diameter 0.755 cm;

(*c*) model body (without flagella) comprising a cylinder of length 4.79 cm and diameter 0.62 cm, with spherically rounded ends;

(*d*) model body, with wire spiralling around the body (axis length of the spiral about 4.5 cm, wavelength about 3.1 cm, diameter of the spiral about 1.5 cm, thickness of the wire 0.02 cm). The wire is fixed on one end of the body. This is an as realistic as possible model of a living *Magnetobacterium bavaricum* (see next section), but without considering the curvature of the body (the scaling factor is approximately 4000);

(*e*) model body, with a straight wire of 4.79 cm length and a thickness of 0.01 cm fixed to one end of the body;

(*f*) model body, with a helical wire fixed to one end of the body: axis length of the spiral about 4.8 cm, wavelength about 2.4 cm, diameter of the spiral about 0.9 cm, thickness of the wire 0.02 cm;

(*g*) model body, with wires (like *d*) on both ends. One of the wires is bent;

(*h*) like (*g*), but both wires are straight.

The wires consisted of constantan and represented flagella or bundles of flagella. In figure 12, the results, normalized to the corresponding ellipsoid, are shown with error estimates and contrasted to numerical results. The errors are calculated in a similar fashion to that explained in §§3.4 and 4.3. However, since we know the shape of the model bacterium very well, and the boundaries are far enough away, we do not have to consider the last two errors in either case, and therefore obtain a smaller total error. One can see, how the resistance factor changes with deviation from the ellipsoidal form (bodies *a* and *b*). More important, however, is the influence of flagella on the resistance factor, especially when they protrude from the body. Except for (*d*), for which the slender-body approximation obviously does not work very well, in all cases the error bars either overlap or almost overlap. However, in every case the numerical calculation gives a smaller resistance factor than the experiment.

4.3. *Discussion of errors*

The total error, which affects the experimental determination of the resistance factors, again comes from a combination of several errors. As before, for each error we give in brackets our best guess:

(*a*) error in the normalization of temperature (0.45%);

(*b*) error due to imperfections in the experimental set-up (originally about 12%; reduced to about 2% due to a greater number of measurements);

(*c*) error due to the one-dimensional approximation (10%);

(*d*) error due to the effect of boundaries (9%);

(*e*) error due to the shape of the bacterium being only known with some uncertainty, so that the model is only an imperfect image of reality (16% – see §3.4 for details).

Assuming that the above errors are independent, we obtain a total error of 21%.

5. Determination of the magnetic moment of real magnetic bacteria

5.1. *Materials and experimental methods*

For the measurements described in the following a special type of magnetic bacterium was selected, which occurs in high abundance in most of the lakes of Southern Bavaria and is named *Magnetobacterium bavaricum.*

The rod-shaped bacterium is about 10 μm long and contains several bundles of chains of magnetosomes (figure 13). The number of magnetosomes in this bacterium

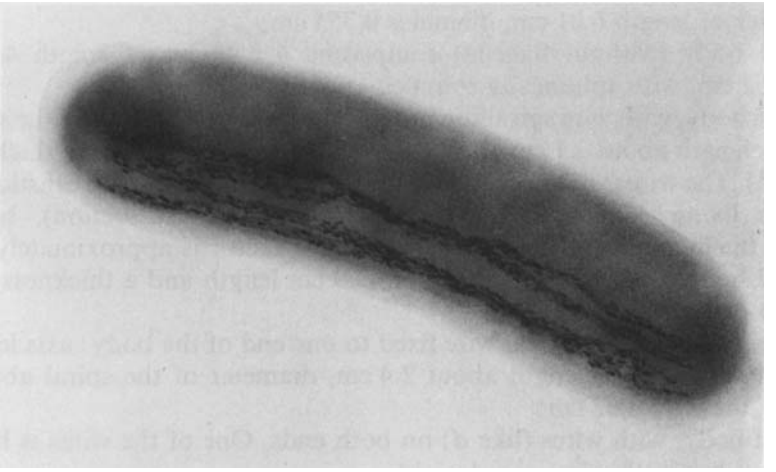

FIGURE 13. Transmission electron micrograph of a magnetic bacterium from Lake Chiemsee with multiple chains of bullet-shaped magnetosomes (*Magnetobacterium bavaricum*). The number of magnetosomes in this type of bacterium is to more than 500.

is more than 500. This is exceptional compared to other magnetic bacteria which usually have 10–50 (for comparison see figure 1 and Blakemore 1982).

The experiments on bacteria in rotating magnetic fields were done in a 'bacteriodrome' (Petersen *et al.* 1989 and Petermann *et al.* 1990), a set-up of two pairs of Helmholtz coils that produces a homogeneous magnetic field at the platform of a light microscope stripped of all of its magnetic parts. The magnetic field rotates in the horizontal plane. The field intensity can be varied between 0 and 10 G, the period of one cycle of rotation being between ∞ (steady field) and 0.5 s.

The bacteria were observed in a chamber of 25 μm thickness made of a cover slip on a glass slide sealed with Valap (vaseline, paraffin, lanolin, 1:1:1). The specimen was observed in brightfield mode with the condenser diaphragm fully closed to reach maximal depth of focus. The C2400 (Hamamatsu Photonics Deutschland, Herrsching FRG) camera control unit was used for analogue contrast enhancement and for analogue shading correction in order to obtain a high-contrast image free of shading (Weiss, Maile & Wick 1989). This was recorded on a video cassette recorder (model VO-5800, Sony Corp.). The recorded sequences were further digitally processed with a real-time image processor (Hamamatsu C1966 Photonic Microscopy System). To visualize the tracks of the bacteria the built-in real-time functions 'rolling average' (over 256 frames) and 'trace' were used. 'Trace' combines self-substraction of images, thereby removing non-motile image elements (sand particles etc.), with an accumulation of each fifth frame in the frame memory. The resulting live video sequences were digitally contrast-enhanced (Weiss *et al.* 1989). Still pictures were obtained by photography from the monitor.

5.2. *Observations relevant to the estimation of the resistance factor F*

First the shape, number and position of the flagellar filaments were determined. For this purpose, the boundary frequency ω_b, up to which the bacteria can follow the rotation of the magnetic field, was measured as a function of the magnetic field H. If the form of the bacterium does *not* depend on the rotation frequency, the relationship

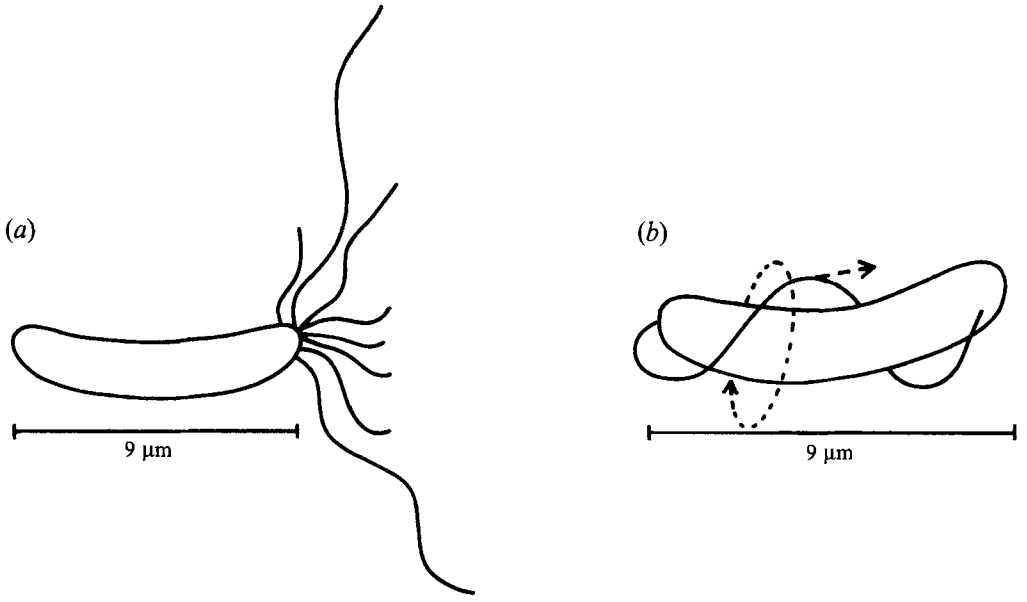

FIGURE 14. Positioning of the flagella in a (*a*) dead and (*b*) a living *Magnetobacterium bavaricum*, as identified by video-enhanced high-resolution light microscopy.

should be approximately $\omega_b \sim B$ (i.e. B/ω_b should be independent of B). If, however, the form changes with increasing rotation frequency, for example if the flagella bend, B/ω_b should decrease with the increasing B since the viscous drag of a bent flagellum is smaller than that of a stiff one.

In the case of *Magnetobacterium bavaricum* we found that B/ω_b decreases as a function of B for dead bacteria, whereas it does not for living bacteria. The reason for this became clear when we observed the bacteria directly by video-enhanced high-resolution light microscopy. With this instrument the flagella can be made visible.

The result of these observations is sketched in figure 14(*a*, *b*). Dead specimens show several flagellar filaments (approximately 8), which all begin at the front end (which refers to the direction of the magnetic field and therefore the forward swimming direction). The flagellar filaments have different lengths: most of them are rather short (about one third of the length of the body), only few (about 1 to 3) are as long as the body. The long filaments seem to be partially waveshaped which means that, in reality, they are helical. These flagellar filaments bend while the bacterium rotates in the magnetic field, and so the resistance factor decreases with increasing rotation frequency.

For microscopic observation of the flagella of the living bacteria we had to slow down the movement by the use of a medium of high viscosity ($\sim$ 15 P). Then it can be seen that all flagella, which are connected to the body at the front end, combine into one bundle. This forms a helix which spirals around the body and rotates when moving forward. One can see only the parts of the helix which are lateral to the body, and which therefore look like 'hooks'. The rotation of the helix appears in the two-dimensional projection as if the 'hooks' were running backward. This interpretation is in accordance with the description of other bacteria which are flagellated only at one end (e.g. Jarosch 1967; Block, Fahrner & Berg 1991) and is also supported by our observation that the resistance factor does not change with the frequency of the rotating magnetic field.

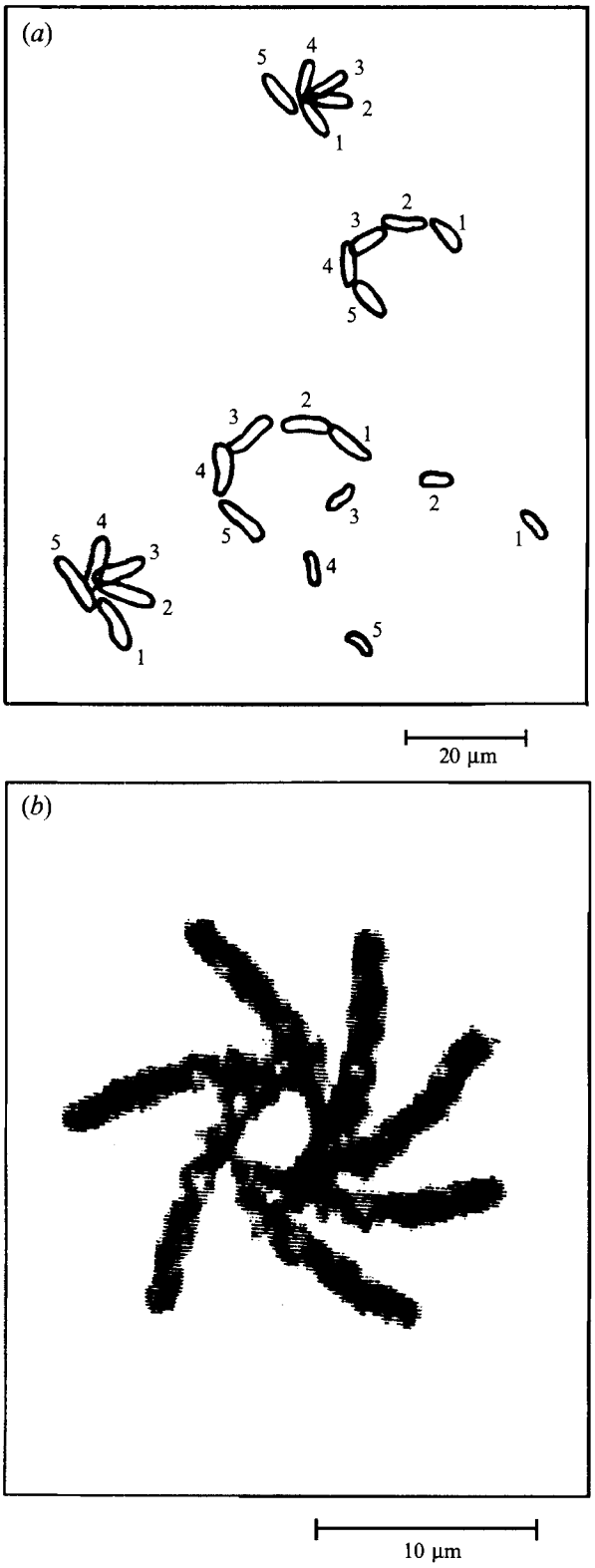

FIGURE 15. For caption see facing page.

	Motion analysis	TEM-observation
Bacterium 1	13 ± 3	16
Bacterium 2	19 ± 4	22
Bacterium 3	64 ± 13	51

TABLE 2. Magnetic moment μ of individual bacteria (*Magnetobacterium bavaricum*) (10^{-12} G cm^3)

We obtain additional proof for the flagella of *Magnetobacterium bavaricum* being fixed at the front end (referring to the forward direction of motion) by comparing the motion of living and dead bacteria in figure 15(*a*). This figure, and figure 15(*b*), were produced by adding several video frames, which succeed each other with a constant time difference in the frame memory of the video microscopy image processor. Here the magnetic field rotates counterclockwise and the living bacteria start swimming towards top left. Now one can compare each position of the living bacteria with the corresponding one of the dead bacteria (figure 15*a*, bottom left and top centre).

We see that the centre of rotation of the dead *M. bavaricum* is asymmetric relative to its body, because of the viscous drag of the flagellar filaments. The comparison of corresponding positions of dead and living bacteria shows then that the flagellum is positioned at the front end (with respect to forward swimming direction). The asymmetry of rotation of a dead *M. bavaricum* is also shown in figure 15(*b*).

5.3. *Results*

When determining the magnetic moment of *M. bavaricum* from the boundary frequency ω_b using equation (3) we have to apply different resistance factors F for dead and living bacteria respectively.

For a dead bacterium the influence of the flagellar filaments on F is high and not well defined (figure 14*a*). The situation is clearer when dealing with a living bacterium (figure 14*b*). For our experiments with living bacteria we chose the experimentally determined resistance factor, which is 1.6 times the resistance factor of an ellipsoid of the same length and width (case *d* in figure 12). The corresponding results are given in table 2. Here the magnetic moment of three different magnetic bacteria, determined by the measurement of the boundary frequency ω_b is listed in the first column.

After determination of ω_b in the bacteriodrome, the respective bacteria were magnetically guided onto a grid for electron microscopy and finally observed under the transmission electron microscope (TEM). The magnetic moment of the bacteria was then calculated from the size and number of magnetosomes as seen in the TEM. This calculation assumes single-domain magnetite particles, with a spontaneous magnetization of 480 G and perfectly parallel alignment of their respective magnetic moments. The results are given in table 2.

The results of the two methods of determination of the bacterial magnetic moment agree very well (taking into account the uncertainty in exactly measuring the volume of the magnestosomes from TEM pictures). The disagreement can be completely explained by the sources of error stated above.

FIGURE 15. (*a*) Motion of dead (top and bottom left) and living *Magnetobacterium bavaricum* in a counterclockwise-rotating magnetic field. Note the asymmetry of rotation of the dead bacteria due to unipolar flagellation from video-enhanced light microscopy in 'trace mode'. From a comparison of corresponding positions of dead and living bacteria it can be deduced that the flagellum is positioned at the front end (with respect to the swimming direction). (*b*) Dead *Magnetobacterium bavaricum*. Magnetic field: 3 Oe, period of rotation: 5.6 s.

6. Conclusions

We have determined resistance factors and boundary frequencies for magnetic bacteria numerically and with a model experiment, as prerequisites for the deduction of the bacterial magnetic moment from motion analysis. Experimental and numerical determination agree within their error bounds.

The resistance factor strongly depends on the number and shape of flagella. The experimental determination of the magnetic moment of real bacteria requires, therefore, observing the magnetic bacterium together with its flagella when it is forced by the external magnetic field to rotate in a liquid of known viscosity. This is possible with the use of video-enhanced microscopy in a bacteriodrome.

We thank W. Maile, Institute of Zoology, Technical University of Munich, for his help with the high-resolution light microscope. Sylvia Chamberlain critically read the manuscript. We are also grateful to the two anonymous reviewers who helped to clarify several issues in the paper. This research was supported by the Deutsche Forschungsgemeinschaft.

REFERENCES

BALKWILL, D. L., MARATEA, D. & BLAKEMORE, R. P. 1980 Ultrastructure of a magnetotactic spirillum. *J. Bact.* **141**, 1399–1408.

BATCHELOR, G. K. 1970 Slender body theory for particles of arbitrary cross-section in Stokes flows. *J. Fluid Mech.* **44**, 419–440.

BLAKEMORE, R. P. 1975 Magnetotactic bacteria. *Science* **190**, 377–389.

BLAKEMORE, R. P. 1982 Magnetotactic bacteria. *Ann. Rev. Microbiol.* **36**, 217–238.

BLAKEMORE, R. P., FRANKEL, R. B. & KALMIJN, A. J. 1980 South-seeking magnetotactic bacteria in the southern hemisphere. *Nature* **286**, 384–385.

BLOCK, S. M., FAHRNER, K. A. & BERG, H. C. 1991 Visualization of bacterial flagella by video-enhanced light microscopy. *J. Bact.* **173**, 933–936.

COX, R. G. 1970 The motion of long slender bodies in a viscous fluid. Part 1. General theory. *J. Fluid Mech.* **44**, 791–810.

COX, R. G. 1971 The motion of long slender bodies in a viscous fluid. Part 2. Shear flow. *J. Fluid Mech.* **45**, 625–657.

DELONG, E. F., FRANKEL, R. B. & BAZYLINSKI, D. A. 1993 Multiple evolutionary origins of magnetotaxis in bacteria. *Science* **259**, 803–806.

EDWARDES, D. 1892 Steady motion of a viscous liquid in which an ellipsoid is constrained to rotate about a principal axis. *Q. J. Maths* **26**, 70–78.

FARINA, M., LINS DE BARROS, H. G. P. & ESQUIVEL, D. M. S. 1988 On the diversity of magnetotactic microorganisms found in natural waters from Brazil. *Inst. Phys. Conf. Ser.* 93: vol. 3, pp. 301–302.

FRANKEL, R. B., BLAKEMORE, R. P., TORRES DE ARAUJO, F. F., ESQUIVEL, D. M. S. & DANON, J. 1981 Magnetotactic bacteria at the geomagnetic equator. *Science* **212**, 1269–1270.

HAPPEL, J. & BRENNER, H. 1965 *Low Reynolds Number Hydrodynamics.* Prentice-Hall.

HIGDON, J. J. L. 1979 A hydrodynamic analysis of flagellar propulsion. *J. Fluid Mech.* **90**, 685–711.

JAROSCH, R. 1967 Studien zur Bewegungsmechanik der Bakterien und Spirochäten des Hochmoores. *Österr. Botanische Z.* **114**, 256–306.

JEFFERY, G. B. 1922 The motion of ellipsoidal particles immersed in a viscous fluid. *Proc. R. Soc. Lond.* A **102**, 161–179.

KELLER, J. B. & RUBINOW, S. I. 1976 Slender-body theory for slow viscous flow. *J. Fluid Mech.* **75**, 705–714.

KIRSCHVINK, J. L. 1980 South-seeking magnetic bacteria. *J. Exp. Biol.* **86**, 345–347.

MACNAB, R. & ORNSTON, M. K. 1977 Normal-to-curly flagellar transitions and their role in bacterial tumbling. *J. Mol. Biol.* **112**, 1–30.

MOENCH, T. T. & KONETZKA, W. A. 1978 A novel method for the isolation and study of a magnetotactic bacterium. *Arch. Microbiol.* **119**, 203–212.

OBERBECK, A. 1876 Ueber stationäre Flüssigkeitsbewegungen mit Berücksichtigung der innernen Reibung. *Crelle* **81**, 62–80.

OBERHACK, M. & SÜSSMUTH, R. 1987 Magnetotactic bacteria from freshwater. *Z. Natur-forsch.* **42c**, 300–306.

PETERMANN, H., WEISS, D. G., BACHMANN, L. & PETERSEN, N. 1990 Motile behaviour and determination of the magnetic moment of magnetic bacteria in rotating magnetic fields. In *Lecture Notes in Biomathematics*, vol. 89 (Biological Motion) (ed. W. Alt & G. Hoffmann), pp. 387–395. Springer.

PETERSEN, N., WEISS, D. G. & VALI, H. 1989 Magnetic bacteria in lake sediments. In *Geomagnetism and Paleomagnetism* (ed. F. Lowes, D. W. Collinson, J. H. Parry *et al.*), pp. 231–241. Kluwer.

PURCELL, E. M. 1977 Life at low Reynolds number. *Am. J. Phys.* **45**, 3–11.

SPARKS, N. H. C., COURTAUX, L., MANN, S. & BOARD, R. G. 1986 Magnetotactic bacteria are widely distributed in sediments in the U.K. *FEMS Microbiol. Lett.* **37**, 305–308.

SPORMANN, A. M. & WOLFE, R. S. 1984 Chemotactic, magnetotactic and tactile behaviour in a magnetic spirillum. *FEMS Microbiol. Lett.* **22**, 171–177.

SPRING, S., AMANN, R., LUDWIG, W., SCHLEIFER, K.-H. & PETERSEN, N. 1992 Phylogenetic diversity and identification of non-culturable magnetotactic bacteria. *Syst. Appl. Microbiol.* **15**, 116–122.

TILLET, J. P. K. 1970 Axial and transverse Stokes flow past slender axisymmetric bodies. *J. Fluid Mech.* **44**, 401–417.

TOWE, K. M. & MOENCH, T. T. 1981 Electron-optical characterization of bacterial magnetite. *Earth Planet. Sci. Lett.* **52**, 213–220.

WEISS, D. G., MAILE, W. & WICK, R. A. 1989 Video microscopy. In *Light Microscopy in Biology* (ed. A. J. Lacey), pp. 1–64 IRL Press-Practical Approach Series, IRL Press Oxford.

WU, T. Y. T., BROKAW, C. J. & BRENNEN, C. (ed.) 1975 *Swimming and Flying in Nature*, vol. 1. Plenum.

YANG, S.-M. & LEAL, L. G. 1983 Particle motion in Stokes flow near a plane fluid–fluid interface. Part 1. Slender body in a quiescent fluid. *J. Fluid Mech.* **136**, 393–421.